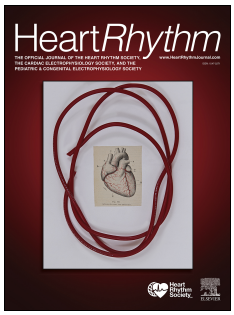

Comparison of Combined Anatomical and Functional Modelling with Purely Anatomical Assessment in Scar-dependent Ventricular Tachycardia

Michael C. Waight, PhD, MBBS, BSc (Hons), MRCP, Adityo Prakosa, PhD, Anthony C. Li, MD (Res), MBBS, BSc (Hons), MRCP, Anh Truong, BSc, Nick Bunce, MD, MBBS, BSc, MRCP, Anna Marciniak, MBBS, PhD, MRCP, Natalia A. Trayanova, PhD, FHRS, FAHA, Magdi M. Saba, MD, MSc, FHRS

PII: S1547-5271(26)00021-4

DOI: https://doi.org/10.1016/j.hrthm.2026.01.006

Reference: HRTHM 11705

To appear in: *Heart Rhythm*

Received Date: 25 September 2025

Revised Date: 15 December 2025

Accepted Date: 3 January 2026

Please cite this article as: Waight MC, Prakosa A, Li AC, Truong A, Bunce N, Marciniak A, Trayanova NA, Saba MM, Comparison of Combined Anatomical and Functional Modelling with Purely Anatomical Assessment in Scar-dependent Ventricular Tachycardia, *Heart Rhythm* (2026), doi: https://doi.org/10.1016/j.hrthm.2026.01.006.

Comparison of Combined Anatomical and Functional Modelling with Purely Anatomical Assessment in Scar-dependent Ventricular Tachycardia

Short title: anatomy vs function + anatomy in VT ablation.

Authors:

1. Michael C Waight; PhD, MBBS, BSc (Hons), MRCP [a, b]
2. Adityo Prakosa; PhD [b]
3. Anthony C Li; MD (Res), MBBS, BSc (Hons), MRCP [a,c]
4. Anh Truong; BSc [b]
5. Nick Bunce; MD, MBBS, BSc, MRCP [c]
6. Anna Marciniak; MBBS, PhD, MRCP [c]
7. Natalia A Trayanova; PhD, FHRS, FAHA [b *]
8. Magdi M Saba; MD, MSc, FHRS [a,c,d *]

* NT and MS are joint senior co-authors.

Authors' affiliations:

a) City St George's, University of London
Cranmer Terrace
London, SW17 0RE
United Kingdom

b) Alliance for Cardiovascular Diagnostic and Treatment Innovation
Johns Hopkins University
3400 N. Charles Street
Baltimore MD 21218

c) St George's University Hospitals NHS Foundation Trust
Blackshaw Road
London, SW17 0QT
United Kingdom
d) Cleveland Clinic London
33 Grosvenor Place
London, SW1X 7HY

Corresponding author:
Dr Michael Waight
City St George's, University of London
Cranmer terrace, London, SW170RE
Email: m2110065@citystgeorges.ac.uk

Conflict of interest: none

Funding

MW received funding through the Advanced Ventricular Arrhythmia Training and Research Project, administered by the St George's Hospital Charity (RES 20 21 001). NT has received grant funding from the National Institutes of Health (R01HL166759 and R01HL174440), National Science Foundation grant DMS-2436738, and a grant from the Leducq Foundation. MS and AL have received modest, restricted grants from Abbott Laboratories.

Clinical Trial Registration Number: NCT04632394

Abstract

Background

Cardiac MRI aids identification of critical substrate in scar-dependent VT. Anatomical assessment (AA) of MRI images detects channels which may sustain VT and are viable targets for ablation. Heart digital twins (DT) combine anatomical data with functional assessment to identify the VT isthmus.

Objective

To assess the additional benefit of combining functional data with anatomy using a DT compared to purely anatomical assessment in identifying critical substrate in ventricular tachycardia (VT).

Methods

18 patients with scar-dependent VT planned for catheter ablation underwent contrast-enhanced cardiac MRI. AA to derive conducting channels was performed. Simultaneously, heart DT models combining personalised heart geometry and functional properties were generated and tested for VT inducibility and optimum ablation lesion sites predicted. Patients underwent invasive VT ablation. Detection of scar and critical substrate was compared between AA and DT.

Results

Scar identification was similar between AA and DT. Total area predicted for ablation was similar between AA and DT (9.94cm^2 [$\pm$ 9.46cm^2] vs 9.84cm^2 [$\pm$ 3.23cm^2], p = 0.96). Sensitivity for detection of abnormal electrograms was greater with DT compared to AA (51.4% [$\pm$ 17.6%] versus 25.3% [$\pm$ 25.4%], p = 0.002). Sensitivity of detection of deceleration zones, mid-diastolic potentials (MDP) and sites of VT termination with ablation was higher with DT than AA, with DT correctly identifying 13/16 (81.3%) of MDP compared to 8/16 by AA (50.0%).

Conclusions

Addition of functional data improves detection of critical substrate above purely anatomical assessment in scar-dependent VT. Digital twins are a potentially useful aid in VT ablation.

Keywords: Ventricular tachycardia, digital twin, anatomical assessment, cardiac MRI, catheter ablation

77

Abbreviations	
AA	Anatomical assessment
CC	Conducting channel
DT	Digital twin
DZ	Deceleration zone
EAM	Electroanatomical map
EGM	Electrogram
FWHM	Full-width half-maximum
ICD	Implantable cardioverter-defibrillator
ICM	Ischaemic cardiomyopathy
ILAM	Isochronal late activation mapping
LGE-MRI	Late gadolinium-enhanced cardiac magnetic-resonance
MDP	Mid-diastolic potential
NICM	Non-ischaemic cardiomyopathy
PSI	Pixel signal intensity
VT	Ventricular tachycardia

78

Introduction

Mapping and ablation of ventricular tachycardia (VT) is a complex procedure, frequently resulting in suboptimal outcomes and high rates of recurrence.[1,2] One of the barriers to successful ablation is accurate estimation of the myocardial scar and definition of the critical components of the VT circuit during tachycardia. Late gadolinium-enhanced cardiac MRI (LGE-MRI) has been used pre-procedurally to aid in planning and guidance of ablation.[3,4]

Recently, technology has been developed which can process the MRI images and provide an automated anatomical assessment (AA), which identifies potential conducting channels (CC) which may sustain VT. Several studies have shown the utility of AA in VT ablation.[5,6] Advantages of this strategy include reduced procedural and fluoroscopy time, with a reduced area of ablation compared to conventional mapping and ablation. Despite promising results, AA is limited to purely anatomical data, with no electrophysiological parameters included in the evaluation.

A novel approach to imaging-guided VT ablation is the combination of anatomical and functional parameters into a personalised heart digital twin (DT), which may help guide ablation. A DT is a virtual construct of a patient's heart which mimics the structure and function of its physical twin in a way which can aid in clinical decision making.[7] DTs have already demonstrated utility in predicting arrhythmogenic risk in patients with both ischaemic and non-ischaemic cardiomyopathy[8,9], identifying substrate abnormalities and VT circuits in scar-VT[10,11] as well as helping understand new mechanisms of arrhythmogenesis.[12] The DT can be tested to demonstrate VT inducibility, and predict optimum ablation lesion targets which can terminate all possible VTs within the model.[8,13] In this study, we assess the additional benefit of modelling, which combines functional and anatomical characteristics of substrate into a DT, over purely AA, in predicting critical substrate and markers of the VT isthmus. Answering this question is critical if an imaging-guided approach to VT ablation is to be pursued in the future.

Methods

Study overview

Prospective patients with ischaemic (ICM) and non-ischaemic (NICM) cardiomyopathy requiring catheter ablation for scar-dependent VT were recruited. Patients underwent pre-procedural 3D LGE-MRI, which was used for AA and DT modelling. AA was used to define scar distribution and location of conducting channels. Imaging-based DTs incorporating electrophysiological properties were used to test arrhythmia inducibility and predict optimum ablation sites which terminate all VTs induced within the model. Patients subsequently underwent invasive VT ablation including substrate and VT activation mapping where possible. The AA and DT models were sequentially merged with the invasively obtained EAM. Substrate abnormalities and markers of the critical VT isthmus were correlated with the AA and DT target sites. Figure 1 shows a schematic overview of the study. Further details of MRI image acquisition, DT modelling and ablation are described in the supplemental materials. The study was granted ethical approval by the Surrey Research Ethics Committee. All patients provided informed consent and the research was carried out in accordance with the Declaration of Helsinki.

Anatomical assessment

Patients underwent requiring catheter ablation for VT underwent pre-procedure 3D LGE-MRI using either a 3T or 1.5T (with wideband sequences) scanner depending on presence of cardiac devices. 3D LGE images were imported into Automatic Detection of Arrhythmogenic Substrate (ADAS 3D, Galgo Medical) and analysed using a validated approach.[14] The left ventricular myocardium was divided into nine sequential layers from endocardium to epicardium to generate nine 3D shells. Tissue characteristics were assigned using the full-width half maximum (FWHM) approach with dense (core) scar being defined as > 50% (± 5%) maximal pixel signal intensity (PSI) and borderzone between 35% (± 5%) and 50% (± 5%) maximal PSI. Tissue with a PSI of less than 35% (± 5%) was

designated as healthy. Conducting channels were identified based on prespecified tissue characteristics derived from the PSI maps and include either channels of borderzone between two areas of dense scar or between dense scar and an anatomical barrier (such as the mitral annulus). CC were defined as endocardial (in layers 10% - 30%), mid (40 - 60%) or epicardial (70 - 90%). Transmural channels were defined by presence in more than 75% of the total myocardial thickness. The AA process was reviewed by an independent observer to ensure consistency.

Digital twin generation

The same 3D LGE-MRI images were used to construct patient-specific digital twins, as described in detail in previous publications[10,12,13,15] and outlined in the supplemental materials. To summarise, endocardial and epicardial boundaries were contoured and voxels underwent thresholding using the FWHM approach[16] based on signal intensity as follows: dense scar (>50% intensity), borderzone (35-50% intensity), and healthy tissue (<35% intensity). These signal thresholding values were chosen for both DT and AA based on previously validated studies using a similar LGE-MRI protocol and are in keeping with our groups previous work.[8–11,13,16–18] Finite-element meshes were created with fibre directionality added using a rule-based approach.[19] Functional electrophysiological properties were then applied to the three tissue regions. Healthy tissue was based on the ten Tusscher ionic model[13], which is based predominantly on human ventricular myocyte studies and was chosen for its balance between model complexity and accurate physiological simulation.[13] Borderzone was assigned modified properties including reduced action potential peak amplitude, longer action potential duration and reduced cell-cell conductivity.[20] Dense scar was modelled as electrically inert. Wavefront propagation was simulated using the opensource software openCARP (https://opencarp.org). Simulated pacing using extrastimuli was applied to 7 left ventricular sites, preferentially targeting scar borderzones, in order to induce re-entry. Once re-entry was observed, simulated ablation lesions were applied to observed VT isthmus sites, rendering them electrically inert with the smallest volume of ablation as possible. Ablation lesions applied in the initial DT within

the native scar substrate were termed “primary sites”. Following application of these lesions, the simulated pacing protocol was re-run to observe for de novo re-entry which may arise in the modified substrate and further simulated ablation lesions were applied to terminate these emergent VTs at “secondary sites”. This process was repeated until the model was rendered non-inducible to VT.

Invasive mapping and ablation protocol

VT ablation was performed under general anaesthesia. Anti-arrhythmic drugs were discontinued 5 half-lives prior to ablation. Electroanatomical mapping was performed with the Advisor HD Grid catheter using Ensite Precision or Ensite X. Substrate mapping was carried out during right ventricular pacing at 600ms. Isochronal late activation maps (ILAM) were generated by annotating the last deflection of the EGMs and dividing the entire ventricular activation period into 8 equal isochrones. Deceleration zones were defined as areas of isochronal crowding with > 3 isochrones within a 1cm radius as previously described.[21] Programmed electrical stimulation from the right ventricle with up to three extrastimuli was used to induce VT. If the induced VT was haemodynamically stable, it was mapped conventionally including entrainment mapping, where possible, at sites of diastolic activity. If the VT was not tolerated, a substrate-based approach to ablation was used. The procedural endpoint was defined as non-inducibility of all induced VTs and ablation of all critical substrate following repeat programmed stimulation.

Critical substrate analysis

Substrate maps were analysed for abnormalities in EGM timing and morphology including EGM onset, offset and total duration which were derived using a bespoke MATLAB runtime. EGMs were visually analysed for abnormalities under the following definitions:

1. Fractionation – EGM with multiple (≥ 4) intrinsic deflections
2. Double potentials – Two discrete deflections separated by an isoelectric interval

3. Late potentials – EGM with a sharp component occurring after the end of the QRS complex
4. Other LAVA – A sharp, high-frequency ventricular potential that is distinct from a preceding or overlapping far-field deflection, not meeting the criteria of any above abnormality

Where VT was induced and sufficiently tolerated for mapping, areas indicative of the critical isthmus were identified based on conventional definitions.[22,23] Areas suggestive of the VT isthmus including mid-diastolic potentials (MDP) observed during activation mapping and, where possible, optimum entrainment characteristics were marked. Sites of termination of VT with ablation were also considered as indicative of the critical isthmus. Sites of isochronal crowding on ILAM were labelled.

Comparison of AA and DT scar size and predicted target characteristics

The exported AA and DT models were sequentially merged with the EAM. Rigid coregistration was performed by an expert independent of subsequent analysis, using landmark fiducial points including the apex, coronary cusps, left ventricular outflow tract and ascending aorta. Total myocardial mass, total scar mass, dense (core) scar area and borderzone area at both endocardial and epicardial surfaces were compared between the AA and the DT. Total myocardial and total scar volume was calculated by converting the total scar volume to mass using 1.05 g/cm^2 as a scaling factor[24] and compared between the assessment methods. Anatomical CC and DT predicted sites were compared in number, distribution, length, width and area. Markers of critical substrate on the EAM, including EGM abnormalities, prolonged EGMs (duration > 70ms)[25,26] and deceleration zones visualised on ILAM, were correlated with CC and DT predicted sites. Markers of the critical VT isthmus during tachycardia, including MDP, optimum entrainment sites and sites of VT termination with ablation, were correlated with CC and DT predicted sites.

Statistical analysis

Continuous, normally distributed data are expressed as mean ± standard deviation. Non-parametric data are expressed as median ± interquartile range. Continuous data were compared using independent samples t-test or Mann-Whitney U test as appropriate. Categorical data were compared using Fisher's exact test or Chi-square test as appropriate. Where comparisons included repeated measures from the same individual, linear mixed models using individuals as random effects were created to compare AA with DT. Pearson's correlation coefficient was used to compare number of anatomical CC and DT predicted sites. Mcnemar's test was used to compare diagnostic performance of AA vs DT. A p value of < 0.05 was taken to indicate statistical significance. Statistical analysis was carried out with SPSS version 30.

Results

Patient demographics

18 patients were recruited. A further 17 were screened but had insufficient LGE-MRI quality to proceed with DT or AA generation and were therefore excluded. Mean age was 68.4 (± 9.5) years. 17/18 (94.4%) were male with a mean baseline left ventricular ejection fraction of 42.3% (± 16.5%). 2/18 patients (11.1%) had had a previous VT ablation. Epicardial mapping was performed in 5/18 (27.8%) of patients. Acute procedural success was seen in 16/18 (88.9%) of patients. Full baseline demographics are listed in Table 1.

Anatomical assessment vs digital twin scar characteristics

Endocardial dense scar area derived from AA was similar to that from DT (33.2 cm^2 [± 22.9 cm^2] vs 29.2 cm^2 [± 13.0 cm^2], p = 0.53). Total myocardial scar mass was 32.7 g (± 28.2 g) for AA and 37.7 g (± 24.7 g) for DT, which was not significantly different (p = 0.41). The proportion of myocardium labelled as scar was similar between AA and DT (23.4% ± [12.2%] vs 25.0% ± [12.1%], p = 0.65). Table 2 shows a comparison of scar assessment between AA and DT.

AA conducting channels vs DT predicted site characteristics

AA generated significantly fewer CC per patient compared to DT predicted (primary and secondary) sites (2.33 [± 1.41] vs 5.11 [± 1.91], p < 0.001). When limiting the comparison to DT primary predicted sites only (those present only in the native substrate), the difference was smaller but there remained fewer CC compared to DT primary predicted sites (2.33 [± 1.41] vs 3.44 [± 1.2], p = 0.02). Compared to DT predicted sites, CC displayed longer length (45.5mm [± 40.3mm] vs 26.0mm [± 10.1mm], p = 0.003) but a similar width (8.08mm [± 2.31mm] vs 7.52mm [± 0.95mm], p = 0.14). The average area of each channel was greater with AA compared to DT (4.17cm^2 [± 5.05cm^2] vs 1.92cm^2 [± 0.70cm^2], p = 0.007).

The total area of myocardium predicted to be of importance per patient was similar with AA compared to DT (9.94cm^2 [± 9.46cm^2] vs 9.84cm^2 [± 3.23cm^2], p = 0.96). The frequency of predictions of epicardial involvement was similar between AA and DT (21/42 [50.0%] vs 40/92 [43.5%], p = 0.58). CC typically involved more AHA segments than DT predicted sites (2.40 [± 1.27) vs 1.47 [± 0.58], p < 0.001). Table 3 shows a comparison of anatomical CC and DT predicted sites. Supplemental Table 1 shows a comparison of CC with DT primary sites only. There was no significant correlation between the number of CC and the number of DT predicted sites per patient (Pearson correlation coefficient = 0.17, p = 0.51) or between the area of CC and the area of DT predicted sites within the same patient (Pearson correlation coefficient = 0.21, p = 0.38).

Spatial distribution and overlap of target sites

The most frequent distribution of both AA and DT target sites was inferior (98/134 [73.1%]) as opposed to anterior (36/134 [26.9%]) and basal (102/134 [76.1%]) as opposed to apical (32/134 [23.9%]). The septal vs lateral distribution of targets was evenly split (68/134 [50.7%] lateral vs 66/134 [49.3%] septal). There was no significant difference in the distribution of the targets between AA and DT as shown in Supplemental Figure 1.

The area of CC which overlapped with DT sites was 45.0% (± 35.0%). Of this overlapping area, 81.8% (± 19.6%) fell into primary DT predictions, whereas 18.4% (± 21.8%) fell into secondary DT predictions. Mean distances from the CC exit and CC mid-section to the nearest DT target site were 9.4mm (± 11.2mm) and 7.8mm (± 10.3mm) respectively. Figure 2 shows a representative group of patients and their respective AA and DT derived scar, conducting channels and DT predicted site.

AA vs DT in predicting presence of EGM abnormalities

During right ventricular pacing, 7487 EGMs were identified within bipolar low voltage (< 1.5mV), of which 2187 (29.2%) were abnormal. Accuracy of AA and DT predicted sites in detecting presence of EGM abnormalities was as follows. Sensitivity of AA was 25.3% (± 25.4%) compared to 51.4% (±

17.6%) for DT (p = 0.002). Specificity of AA was 70.7% (± 30.4%) compared to 70.1% (± 17.5%) for DT (p = 0.94). Positive predictive value of AA was 28.6% (± 19.9%) compared to 45.4% (± 16.3%) for DT (p = 0.006). Negative predictive value of AA was 64.2% (± 25.7%) compared to 76.8% (± 10.3%) for DT (p = 0.03). 3234/7487 (43.2%) of EGMs within bipolar low voltage were prolonged (>70ms duration). Accuracy of AA and DT in detecting the presence of prolonged EGMs at predicted sites was as follows. Sensitivity of AA was 21.6% (± 22.7%) compared to 50.8% (± 22.1%) for DT (p = 0.002) Specificity of AA was 81.8% (± 19.1%) compared to 71.6% (± 17.8%) for DT (p = 0.10). Positive predictive value of AA was 37.3% (± 30.8%) compared to 56.6% (± 21.2%) for DT (p = 0.004). Negative predictive value of AA was 60.6% (± 17.6%) compared to 67.1% (± 20.6%) for DT (p = 0.02). Comparative accuracy of AA and DT for predicting abnormal and prolonged EGMs is shown in Figure 3.

Predictive accuracy of AA vs DT for ILAM deceleration zone identification

26 deceleration zones were identified during right ventricular pacing. The mean distance of each DZ from the closest anatomical CC and DT predicted site were 13.86mm (± 20.41mm) and 5.39mm (± 9.45mm) respectively. DZ were more frequently located within 5 mm of a DT predicted site compared to an CC (21/26 [80.77%] vs. 14/26 [53.8%] respectively, p = 0.03). Of the 21 DZ located at a DT predicted site, 14/21 (66.7%) were closest to a primary site and 7/21 (33.3%) were located closest to a secondary site. Of the 14 DZ identified by AA, 12/14 (85.7%) were also detected by DT. Of these, 10/12 (83.3%) were located at primary DT sites and 2/12 (16.7%) were located at secondary DT sites. Figure 4 demonstrates a patient with ischaemic cardiomyopathy and lateral wall scar where both a CC and a DT predicted site co-located to an area of slow conduction, identified by ILAM.

AA vs DT in predicting diastolic activity and sites of termination with ablation

Monomorphic VT was inducible in 15/18 (83.3%) patients. The total number of induced VTs was 43 with a mean of 2.4 (range 0-6) VTs induced per patient. Mid-diastolic activity was detected during activation mapping in 16/43 (37.2%) VTs. 8/16 MDP sites were located at an anatomical CC compared to 13/16 MDP sites located at a DT predicted site. The sensitivity of detection of diastolic activity was significantly higher with DT compared to AA (81.3% vs 50.0%, $p = 0.02$). In all eight cases where the MDP were detected by AA they were also detected by DT. Importantly, in 6/8 (75.0%) cases the overlap was with a DT primary predicted site as opposed to a secondary site. Equally, of the five cases where DT correctly predicted the site of MDP, but AA did not, the DT site was a primary site in 4/5 (80.0%) cases.

Due to haemodynamic instability and termination of tachycardia, entrainment was possible in only 4/16 VTs where diastolic activity was detected. Of these, fusion was concealed in 3/4 cases (75%) and manifest in 1/4 cases (25%). These concealed entrainment sites were correctly identified by AA in 2/3 (66.7%) cases compared to 3/3 (100%) of cases by DT. Termination with ablation was achieved in 5 cases, of which the termination site was located at a CC in 3/5 (60.0%) cases and at a DT predicted site in 4/5 (80%) cases. Where epicardial mapping was performed (5/18 cases), the VT was mapped to the epicardium in 1/5 (20%) cases. Figure 5 shows an example of a patient with ICM and epicardial lateral wall scar. A sustained VT was mapped to the borderzone of this scar. Overlaying CC and DT predicted sites showed superior predictivity of DT for the critical isthmus. Termination with ablation was achieved directly beneath a DT predicted site, but distant from the AA conducting channel.

Discussion

The aim of this study was to compare the predictive accuracy of two emerging techniques, based on cardiac imaging, in predicting critical substrate for scar-dependent VT ablation. One technique uses purely anatomical data, while the other combines functional parameters with anatomy. This is the first study to systematically compare the two modalities, and we demonstrated the superiority of a combined functional and anatomical approach in predicting critical substrate in VT.

Minimising burden of ablation

Re-entrant VT is dependent on the size and morphology of the myocardial scar, and, in order to be of clinical value, any scar-analysis technology must accurately differentiate dense scar and borderzone from healthy tissue. Regardless of whether purely anatomical assessment or combined anatomical and functional assessment was carried out, scar segmentation was performed using the same technique. As a consequence, and as expected, scar quantification was not significantly different between AA and DT. In our study, both modalities used the same FWHM technique and threshold for dense scar and borderzone quantification, resulting in consistent scar characterisation between the modalities and allowing for fair comparison. CC tended to be of longer length, similar width, and overall larger area than DT predicted sites. As a product of the DT methodology, combined anatomical plus functional modelling tends to generate more numerous targets than AA and consequently the total area of myocardium predicted to be of importance was similar between the two modalities. We suggest that the shorter length and smaller area of individual DT predicted sites compared to CC is due to the fact that the DT targets only the isthmus of a VT site, where a short ablation lesion is sufficient to interrupt conduction, whereas an anatomical channel may include the VT entrance, isthmus and exit along its entire length. Ablation at any point along this channel may theoretically terminate the VT.

One significant advantage of DT over AA in this regard is the ability of the DT to predict not only VTs which may arise in the initial substrate, but also, through an iterative process, VTs which might emerge as a consequence of the application of the primary ablation lesion set. This repeated testing of the modified substrate represents the hallmark of our DT technology and there is an expectation that the risk of recurrence is therefore reduced. Consequently, the DT predicted sites represents a more efficient set of ablation targets compared to AA, which only assesses the primary substrate. However, it must be remembered that in the clinical setting, the predictivity of post-ablation VT inducibility on long-term recurrence remains uncertain.[27]

The overlap between CC and DT predicted sites was around 50%, with the vast majority of the overlap being with DT primary predicted sites. This is logical since AA does not simulate electrical propagation or analyse the influence of ablation of the initial set of conducting channels. We suggest that the moderate overlap is likely to represent the importance of anatomy to both techniques, though the addition of functional properties to the substrate makes it possible that an anatomical corridor is unable to sustain re-entry once factors such as conduction velocity and cell-cell conductivity are taken into consideration.

Are VT isthmuses functional or anatomical?

Traditional dogma suggests that a VT isthmus consists of both anatomical and functional components. The former is represented by bundles of surviving myocytes through an area of non-conducting scar[28] and its distribution entirely dependent on the tissue anisotropy and fibrosis resulting from an infarct or other form of injury. By contrast, functional changes range from sub-normal conduction to block depending on a variety of factors and are characterised by regions of fractionated and delayed EGMs or decremental conduction on extrastimulation.

In our analysis, we observed that the addition of functional properties to anatomical data led to a greater sensitivity to both abnormal and prolonged EGMs, whilst maintaining a high specificity. Both abnormal and prolonged EGMs present valid targets for ablation in scar-dependent VT[29,30],

particularly for those in whom mapping during VT is not possible. Of perhaps greater significance is the finding of stronger association of DT predicted sites than CC with MDP, optimum entrainment sites, sites of termination with ablation, and deceleration zones all of which are markers of the critical isthmus or reentry-prone sites and represent the gold standard targets for VT ablation.

DT offers the potential to visualise likely areas of conduction slowing and eventual electrical turnaround and reentry, which may account for the superior predictivity of DT over AA in this analysis. Most of the detection of DZ and MDP was by primary DT predicted sites. Whether the secondary sites are of significance for recurrent VT is uncertain and requires further evaluation.

Implications for DT-guided VT ablation

Personalised, imaging-based technology which can accurately predict the likely location of re-entry in scar VT has potential to aid procedural planning, reduce ablation time and prevent arrhythmia recurrence. It may even be considered to directly guide ablation, obviating the requirement for electroanatomical mapping. LGE-MRI is the most commonly used modality to assess scar and has been shown to improve outcomes for patients undergoing VT ablation.[5,31] With the addition of functional properties over and above personalised cardiac anatomy, the diagnostic performance of image-based modelling can be significantly improved, whilst simultaneously offering the potential to reduce VT recurrence and reduce procedural complications through reduced procedural time. These technologies offer a useful tool to the electrophysiologist to help guide VT ablation.

Limitations

This was a single-centre study with a small patient cohort, predominantly in an ICM cohort. This is due to the strict quality control over the 3D LGE-MRI scan required for the assessment described. Both AA and DT rely on acquiring artefact-free 3D LGE-MRI, which can be especially challenging in patients with ICDs. The computational resources and time required for DT modelling are high. AA is more readily available but still requires a financial commitment as well as an experienced technician

to process the images. As software developments and advances in machine learning continue, it is reasonable to expect that the time and resource requirements for both modalities will fall in due course. Furthermore, alternative imaging modalities such as cardiac CT show promise in their ability to provide modelling data.[12,18,32] Merging of the MRI is subject to coregistration errors, which can influence the comparison with the EAM. Channel identification by either AA or DT is dependent on signal thresholding values,[33] which may influence the agreement with invasive findings.

Conclusion

The addition of MRI-based functional data and digital twin simulation over a purely anatomical assessment results in improved detection of critical substrate in scar-VT. Heart digital twins offer a personalised model which may improve precision and outcomes in VT ablation.

References

1. Liang JJ, Santangeli P, Callans DJ: Long-term Outcomes of Ventricular Tachycardia Ablation in Different Types of Structural Heart Disease. Arrhythmia & Electrophysiology Review, 2015; 4:177.

2. Al-Khatib S, Daubert J, Anstrom K, et al.: Catheter ablation for ventricular tachycardia in patients with an implantable cardioverter defibrillator (CALYPSO) pilot trial. Journal of cardiovascular electrophysiology, 2015; 26:151–157.

3. Dickfeld T, Tian J, Ahmad G, et al.: MRI-Guided Ventricular Tachycardia Ablation. Circulation: Arrhythmia and Electrophysiology, 2011; 4:172–184.

4. Piers SRD, Tao Q, De Riva Silva M, et al.: CMR–Based Identification of Critical Isthmus Sites of Ischemic and Nonischemic Ventricular Tachycardia. JACC: Cardiovascular Imaging, 2014; 7:774–784.

5. Soto-Iglesias D, Penela D, Jáuregui B, et al.: Cardiac Magnetic Resonance-Guided Ventricular Tachycardia Substrate Ablation. JACC Clinical electrophysiology, 2020; 6:436–447.

6. Andreu D, Penela D, Acosta J, et al.: Cardiac magnetic resonance–aided scar dechanneling: Influence on acute and long-term outcomes. Heart Rhythm, 2017; 14:1121–1128.

7. National Academies of Sciences E and M: Foundational Research Gaps and Future Directions for Digital Twins. Foundational Research Gaps and Future Directions for Digital Twins, 2023; .

8. Arevalo HJ, Vadakkumpadan F, Guallar E, et al.: Arrhythmia risk stratification of patients after myocardial infarction using personalized heart models. Nature Communications, 2016; 7.

9. Zhang Y, Zhang K, Prakosa A, et al.: Predicting Ventricular Tachycardia Circuits in Patients with Arrhythmogenic Right Ventricular Cardiomyopathy using Genotype-specific Heart Digital Twins. eLife, 2023; 12.

10. Waight MC, Prakosa A, Li AC, et al.: Personalized Heart Digital Twins Detect Substrate Abnormalities in Scar-Dependent Ventricular Tachycardia. Circulation, 2025; 151.

11. Waight MC, Prakosa A, Li AC, et al.: Heart Digital Twins Predict Features of Invasive Reentrant Circuits and Ablation Lesions in Scar-Dependent Ventricular Tachycardia. Circulation: Arrhythmia and Electrophysiology, 2025; 18:13660.

12. Sung E, Prakosa A, Zhou S, et al.: Fat infiltration in the infarcted heart as a paradigm for ventricular arrhythmias. Nature cardiovascular research, 2022; 1:933–945.

13. Prakosa A, Arevalo HJ, Deng D, et al.: Personalized virtual-heart technology for guiding the ablation of infarct-related ventricular tachycardia. Nature Biomedical Engineering, 2018; 2:732–740.

14. Andreu D, Ortiz-Pérez JT, Fernández-Armenta J, et al.: 3D delayed-enhanced magnetic resonance sequences improve conducting channel delineation prior to ventricular tachycardia ablation. Europace : European pacing, arrhythmias, and cardiac electrophysiology : journal of the working groups on cardiac pacing, arrhythmias, and cardiac cellular electrophysiology of the European Society of Cardiology, 2015; 17:938–945.

15. Shade JK, Cartoski MJ, Nikolov P, et al.: Ventricular arrhythmia risk prediction in repaired Tetralogy of Fallot using personalized computational cardiac models. Heart Rhythm, 2020; 17:408–414.

16. Schmidt A, Azevedo CF, Cheng A, et al.: Infarct Tissue Heterogeneity by Magnetic Resonance Imaging Identifies Enhanced Cardiac Arrhythmia Susceptibility in Patients With Left Ventricular Dysfunction. Circulation, 2007; 115:2006–2014.

17. Mesubi O, Ego-Osuala K, Jeudy J, et al.: Differences in quantitative assessment of myocardial scar and gray zone by LGE-CMR imaging using established gray zone protocols. International Journal of Cardiovascular Imaging, 2015; 31:359–368.

18. Sung E, Prakosa A, Aronis KN, et al.: Personalized Digital-Heart Technology for Ventricular Tachycardia Ablation Targeting in Hearts With Infiltrating Adiposity. Circulation: Arrhythmia and Electrophysiology, 2020; 13:E008912.

19. Bayer JD, Blake RC, Plank G, Trayanova NA: A novel rule-based algorithm for assigning myocardial fiber orientation to computational heart models. Annals of biomedical engineering, 2012; 40:2243–2254.

20. Arevalo H, Plank G, Helm P, Halperin H, Trayanova N: Tachycardia in post-infarction hearts: insights from 3D image-based ventricular models. PloS one, 2013; 8.

21. Irie T, Yu R, Bradfield JS, et al.: Relationship between sinus rhythm late activation zones and critical sites for scar-related ventricular tachycardia. Circulation: Arrhythmia and Electrophysiology, 2015; 8:390–399.

22. Stevenson WG, Soejima K: Catheter ablation for ventricular tachycardia. Circulation, 2007; 115:2750–2760.

23. De Chillou C, Lacroix D, Klug D, et al.: Isthmus characteristics of reentrant ventricular tachycardia after myocardial infarction. Circulation, 2002; 105:726–731.

24. Buechel EV, Kaiser T, Jackson C, Schmitz A, Kellenberger CJ: Normal right- and left ventricular volumes and myocardial mass in children measured by steady state free precession cardiovascular magnetic resonance. Journal of Cardiovascular Magnetic Resonance, 2009; 11:19.

25. Cassidy DM, Vassallo JA, Buxton AE, Doherty JU, Marchlinski FE, Josephson ME: The value of catheter mapping during sinus rhythm to localize site of origin of ventricular tachycardia. Circulation, 1984; 69:1103–1110.

26. Masjedi M, Jungen C, Kuklik P, et al.: A novel algorithm for 3-D visualization of electrogram duration for substrate-mapping in patients with ischemic heart disease and ventricular tachycardia. PloS one, 2021; 16.

27. Sipko J, Baranowski B, Bhargava M, et al.: Acute post-procedural inducibility is a poor predictor of clinical outcomes in high-risk patients (PAINESD > 17) undergoing scar-related ventricular tachycardia ablation. EP Europace, 2024; 26:185.

28. De Bakker JMT, Janse MJ, Van Capelle FJL, Durrer D: Endocardial mapping by simultaneous recording of endocardial electrograms during cardiac surgery for ventricular aneurysm. Journal of the American College of Cardiology, 1983; 2:947–953.

29. Nakahara S, Tung R, Ramirez RJ, et al.: Distribution of late potentials within infarct scars assessed by ultra high-density mapping. Heart rhythm, 2010; 7:1817–1824.

30. Rossi P, Cauti FM, Niscola M, et al.: Ventricular Electrograms Duration Map to Detect Ventricular Arrhythmia Substrate: the VEDUM Project Study. Circulation: Arrhythmia and Electrophysiology, 2023; 16:447–455.

31. Andreu D, Penela D, Acosta J, et al.: Cardiac magnetic resonance-aided scar dechanneling: Influence on acute and long-term outcomes. Heart rhythm, 2017; 14:1121–1128.

32. Cedilnik N, Duchateau J, Dubois R, et al.: Fast personalized electrophysiological models from computed tomography images for ventricular tachycardia ablation planning. EP Europace, 2018; 20:iii94–iii101.

33. Burger JC, Hopman LHGA, Campos FO, et al.: Optimizing ventricular scar characterization in late-gadolinium enhancement cardiac MRI: Impact of thresholding techniques in magnitude and phase-sensitive reconstructed images. Heart rhythm, 2025;

Tables

Table 1: Baseline demographics of the cohort.

	ICM (15)	**NICM (3)**	**Total (18)**
Age (years)	67.7 (± 9.7)	71.7 (± 7.4)	68.4 (± 9.5)
Male gender	14 (93.3%)	3 (100%)	17 (94.4%)
Baseline LVEF (%)	41.5 (± 17.7)	46.3 (± 10.0)	42.3 (± 16.5)
NYHA class			
I	7 (46.6%)	1(33.3%)	8 (44.4%)
II	5 (33.3%)	2 (66.7%)	7 (38.9%)
III	3 (20.0%)	0	3 (16.7%)
IV	0	0	0
Hypertension	11 (73.3%)	2 (66.7%)	13 (72.2%)
Diabetes	6 (40.0%)	1 (33.3%)	7 (38.9%)
Atrial fibrillation	6 (40.0%)	2 (66.7%)	8 (44.4%)
Chronic kidney disease	7 (46.7%)	2 (66.7%)	9 (50.0%)
Beta-blocker	14 (93.3%)	3 (100%)	17 (94.4%)
Amiodarone	4 (26.7%)	3 (100%)	7 (38.9%)
Mexiletine	2 (13.3%)	1 (33.3%)	3 (16.7%)
ICD	12 (80.0%)	3 (100%)	15 (83.3%)
CRT-D	2 (10.7%)	0	2 (11.1%)
Prior VT ablation	2 (13.3%)	0	2 (11.1%)
Epicardial mapping	3 (16.7%)	2 (66.7%)	5 (27.8%)
Procedural success	14 (93.3%)	2 (66.7%)	16 (88.9%)

ICM = ischaemic cardiomyopathy, NICM = non-ischaemic cardiomyopathy. LVEF = left ventricular ejection fraction, ICD = implantable cardioverter-defibrillator, CRT-D = cardiac resynchronisation therapy-defibrillator.

Table 2: Comparison of AA vs DT scar assessment

	AA	**DT**	**p – value**
Endocardial dense scar area (cm^2)	33.2 (± 22.9)	29.2 (± 13.0)	0.53
Endocardial borderzone area (cm^2)	46.3 (± 20.2)	42.0 (± 13.6)	0.50
Epicardial dense scar area (cm^2)	54.4 (± 55.9)	52.2 (± 31.9)	0.94
Epicardial borderzone area (cm^2)	61.6 (± 26.5)	62.7 (± 31.8)	0.95
Total myocardial mass (g)	137.4 (± 52.1)	151.3 (± 65.4)	0.36
Total myocardial scar mass (g)	32.7 (± 28.2)	37.7 (± 24.7)	0.41
% of myocardium labelled as scar	23.4 (± 12.2)	25.0 (± 12.1)	0.65

AA = anatomical assessment, DT = digital twin

Table 3: Comparison of anatomical conducting channels vs DT predicted site characteristics.

	AA (n = 42)	**DT (n = 92)**	**P – value**
Number per patient	2.33 (± 1.41)	5.11 (± 1.91)	< 0.001
Length per channel/site (mm)	45.5 (± 40.3)	26.0 (± 10.1)	0.003
Width per channel/site (mm)	8.08 (± 2.31)	7.52 (± 0.95)	0.14
Area per channel/site(cm^2)	4.17 (± 5.05)	1.92 (± 0.70)	0.007
Total area predicted per patient	9.94 (± 9.46)	9.84 (± 3.23)	0.96
Epicardial isthmus	21 (50.0%)	40 (43.5%)	0.58
No of AHA segments involved	2.40 (± 1.27)	1.47 (± 0.58)	< 0.001
EAM map density (points/cm^2)	42.3 (± 30.3)	39.0 (± 11.0)	0.69

AA = anatomical assessment, DT = digital twin, AHA = American Heart Association, EAM = electroanatomical map.

Figure legends

Figure 1: **Study Overview**

3D LGE-MRI images are acquired from patients undergoing VT ablation. MRI images are used to generate anatomical scar and conducting channel maps (top row). Concurrently, 3D LGE-MRI images are used to generate a digital twin, in which VT is simulated through rigorous pacing protocols and optimum ablation lesions to terminate the VTs are derived (bottom row). The anatomical assessment and digital twin are in turn merged with the EAM following invasive VT ablation and characteristics of the predictions are compared.

Figure 2: Example of AA and DT outputs from 5 patients.

Top row demonstrates the AA derived conducting channels (white areas) which traverse the borderzone regions. Second row demonstrates DT predicted sites (blue). Third row demonstrates the AA derived scar distribution. The bottom row represents the DT derived scar distribution. Note close correlation between anatomical CC and DT predicted sites in patients A, B and C. Contrast with poorer correlation for patients D and E.

Figure 3: Diagnostic performance of AA conducting channels and DT predicted sites

Detection of presence of abnormal EGMs (A) and prolonged EGMs (duration > 70ms) (B) within low voltage areas (<1.5mV). * denotes statistical significance.

Figure 4: Patient with ischaemic cardiomyopathy with basal lateral wall scar where DT predictions and AA channels co-locate closely and lie along a deceleration zone.

A: voltage map demonstrating extensive lateral wall scar. MRI scar from AA (B) and DT (C) matches EAM. D – isochronal late activation map shows deceleration zone (white circle) at mid-apical lateral wall, on the scar border. E: CC shown in grey with yellow border and F: DT predicted sites shown in red with yellow border. Note both CC and DT predicted sites co-locate to deceleration zone and show spatial overlap.

Figure 5: Example of superior prediction by DT compared to AA.

A – epicardial voltage map showing basal to mid inferolateral and lateral wall scar. B – VT activation map demonstrating potential isthmus (purple borders). C – ablation catheter located at putative isthmus with DT predicted sites (white star) and anatomical CC (yellow arrows) overlaid shows better identification of critical site by DT. D – VT slowing and termination with ablation at DT predicted site.

3D LGE-MRI

Image analysis

Merge with EAM

Comparison

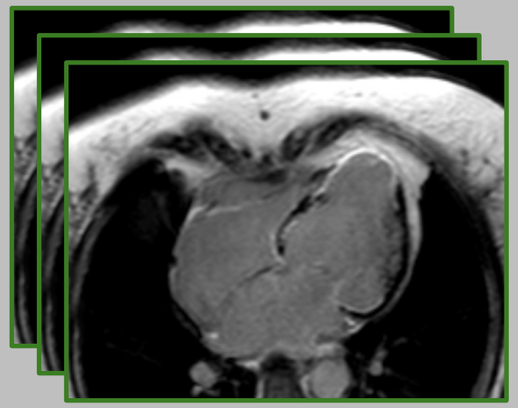

ADAS: anatomical assessment

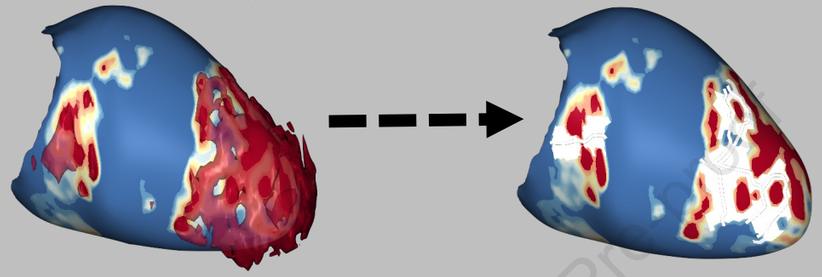

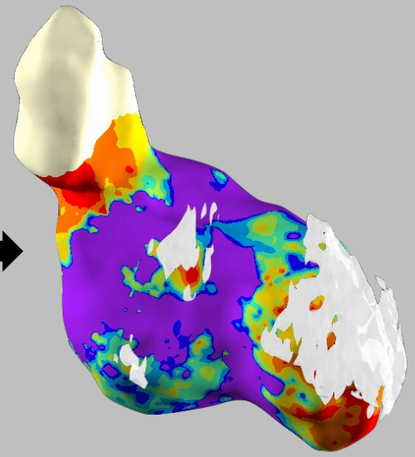

VT Simulation

Ablation

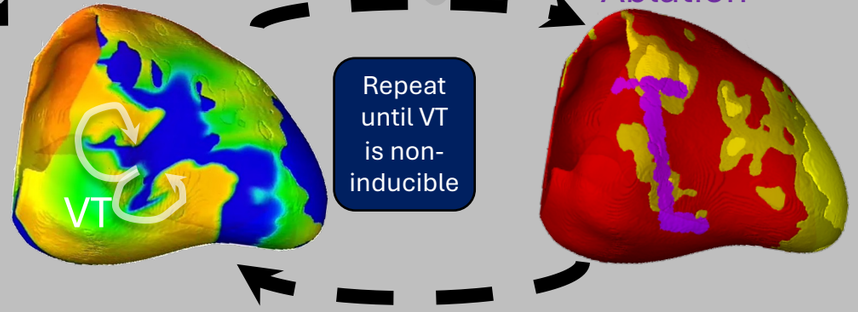

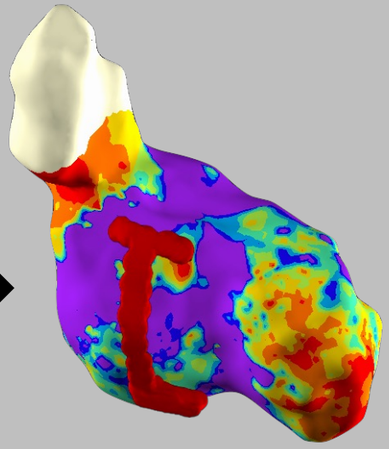

Digital twin: functional + anatomical modelling

- Scar size
- Predicted target characteristics
- Prediction of:
  - Abnormal EGMs
  - Prolonged EGMs
  - Deceleration zones
  - Diastolic activity in VT
  - Sites of VT termination with ablation

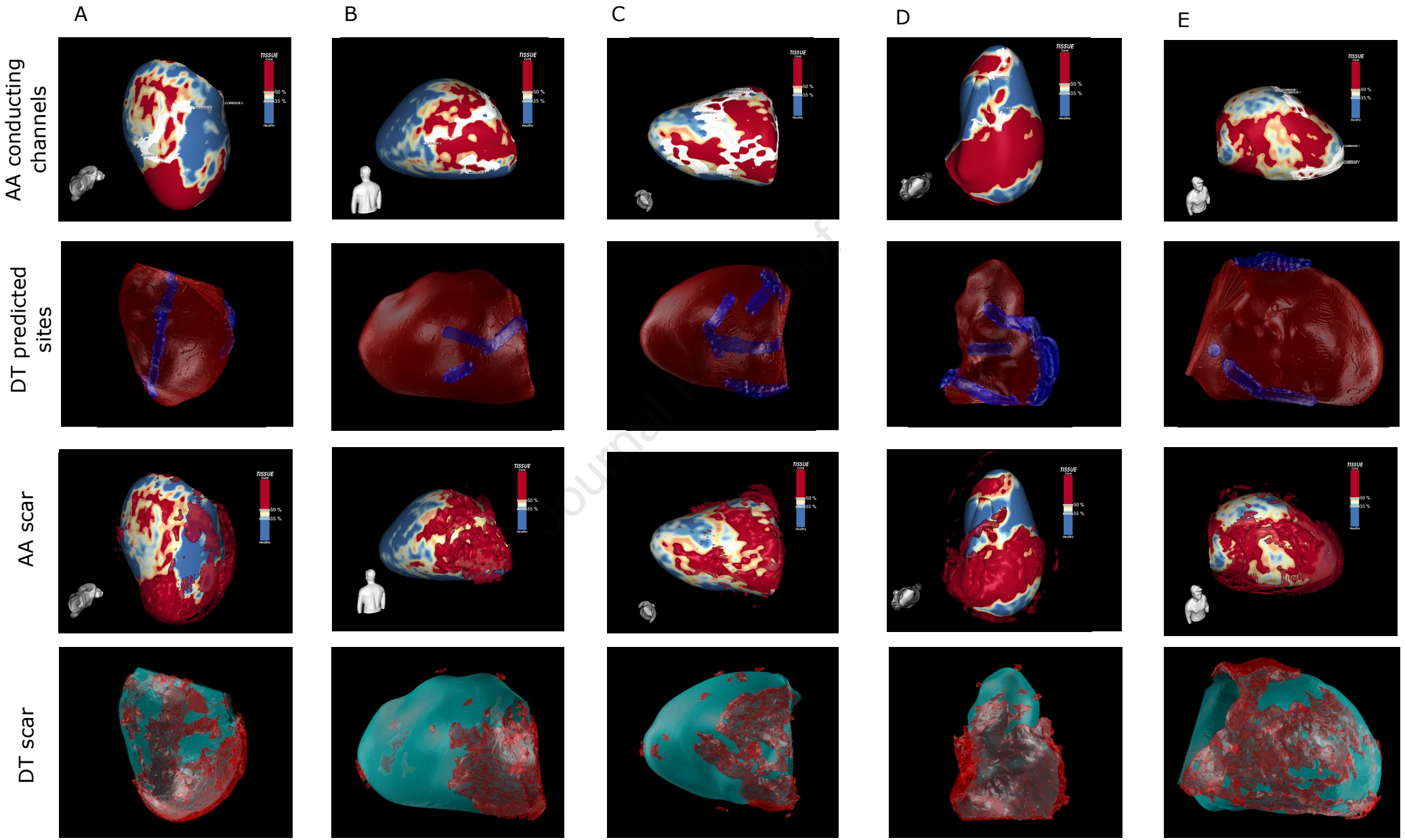
A
B
C
D
E
AA conducting channels
DT predicted sites
AA scar
DT scar
TISSUE
Core
50 %
35 %
Healthy

A

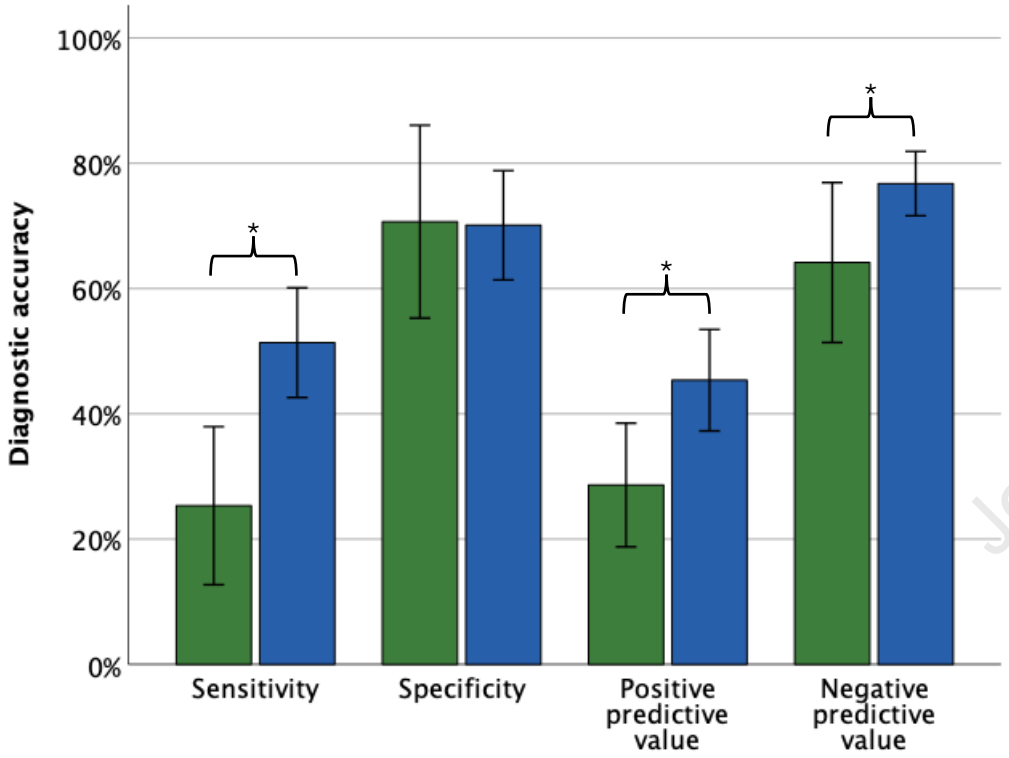

B

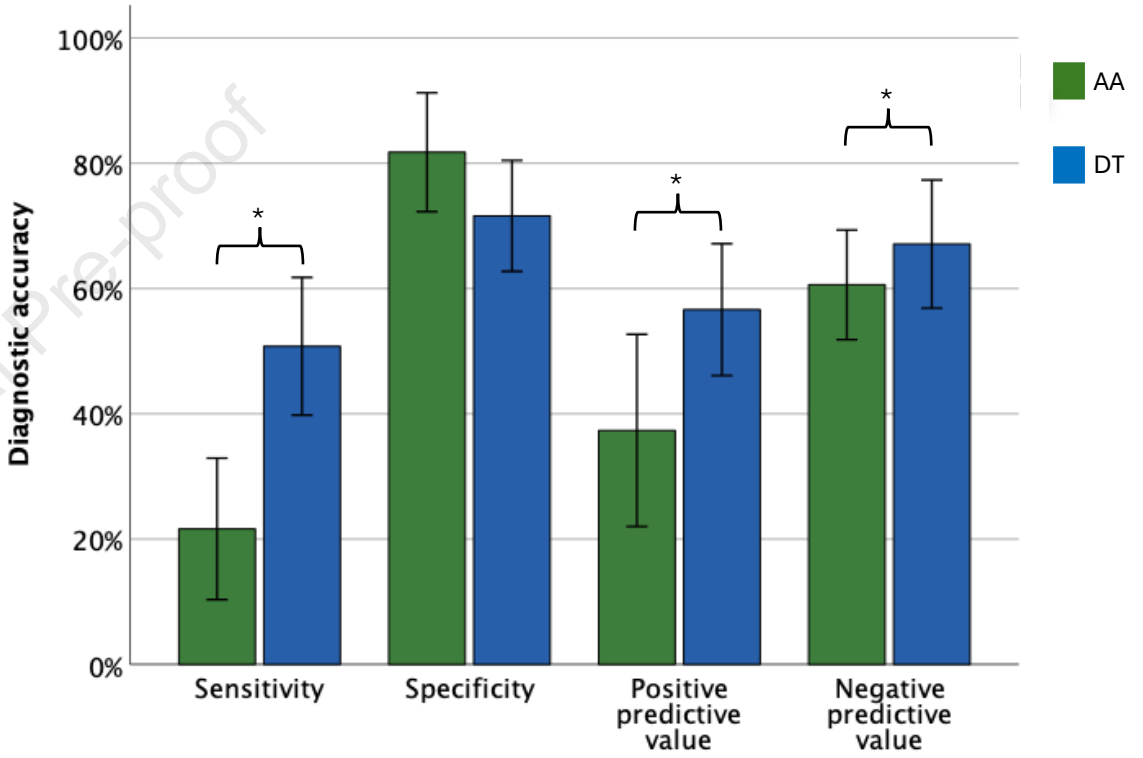

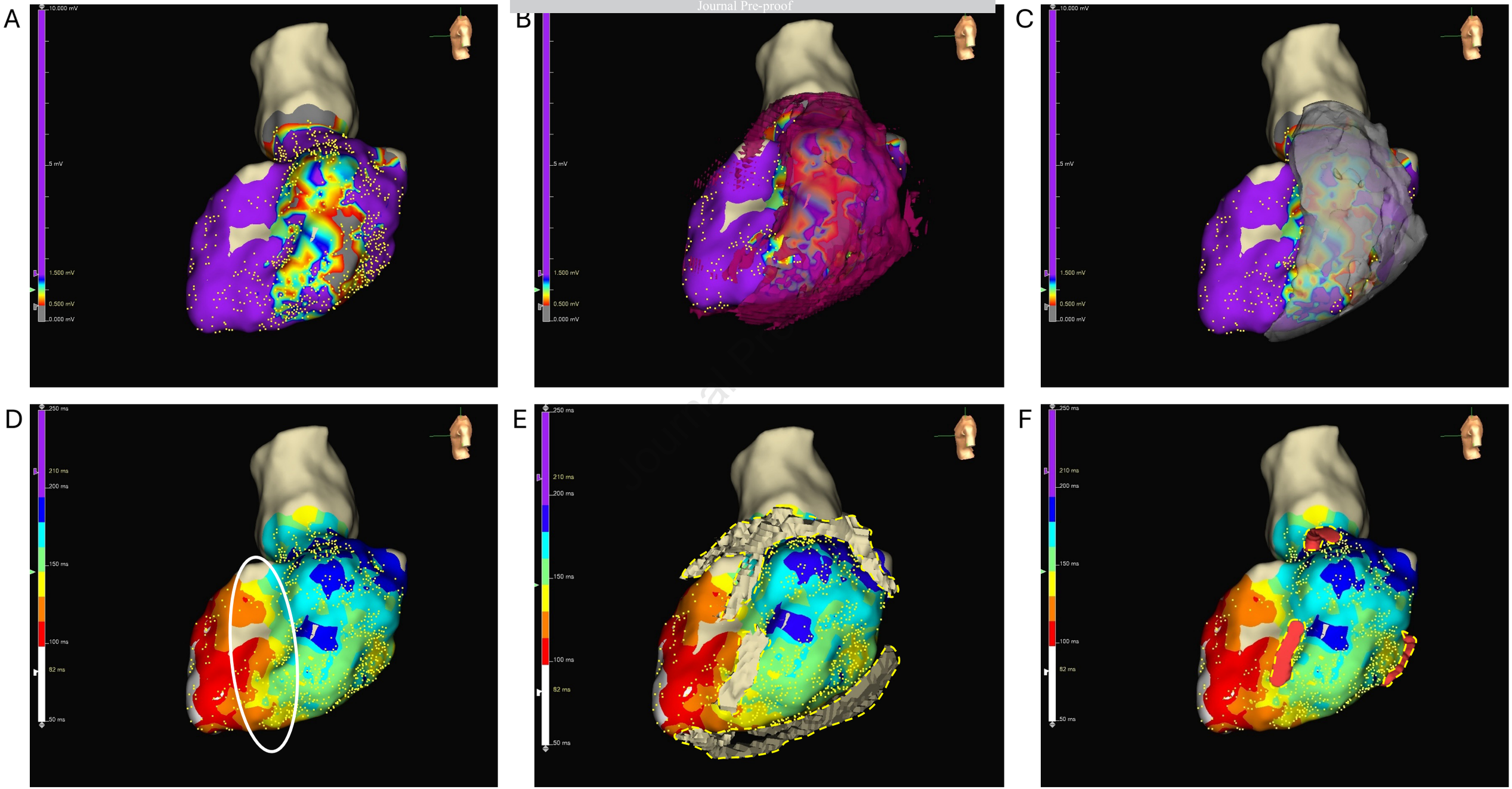

A

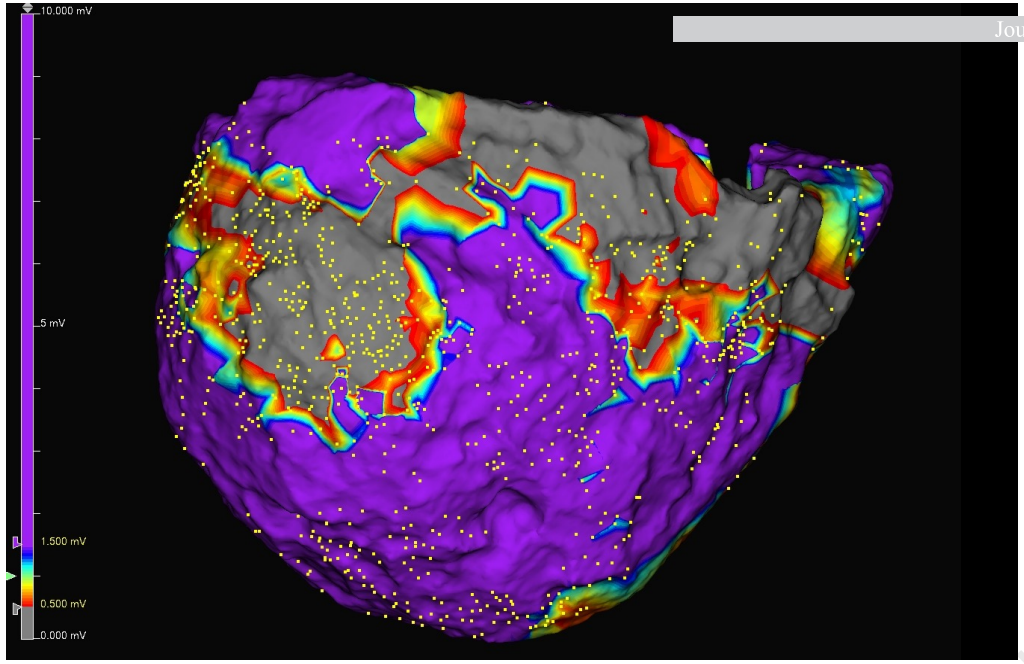

B

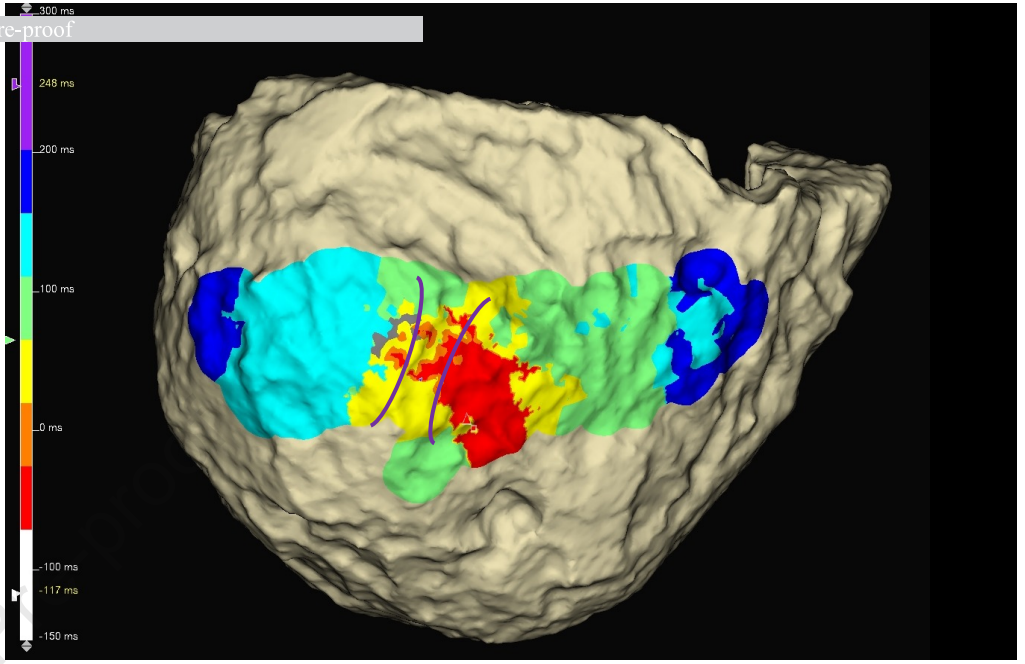

C

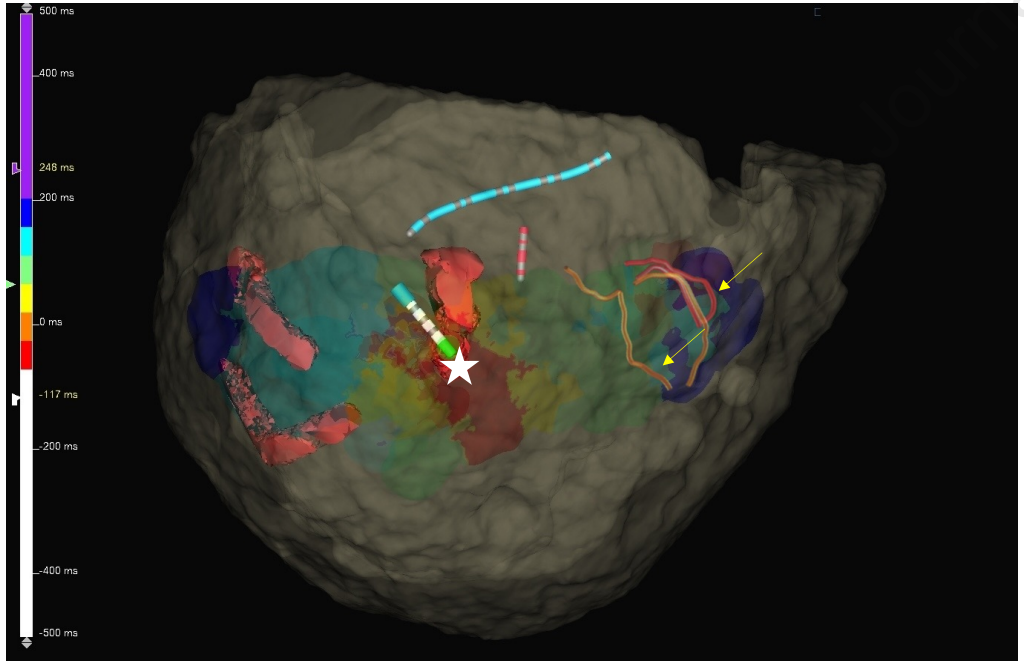

D

Supplemental materials

MRI acquisition

Cardiac MRI was performed using a 3T Philips Achieva magnet (Philips Healthcare, Best, Netherlands) and a 32 channel coil for patients without an ICD or CRT. A Siemens Magnetom Aera 1.5T magnet (Siemens, Munich, Germany) with wideband sequences was used in those with an ICD or CRT. Standard sequences were obtained during breath-holds using white blood steady state free precession sequences (SSFP) and black blood turbo spin echo (TSE), with ECG signal gating.

In addition, a 3D LGE enhanced sequence was obtained following the standard images. Images were obtained 8-10 minutes following the administration of a 0.15mmol/kg intravenous bolus of gadobutrol (Gd-BT-DO3A) (Gadovist). The optimal inversion time (TI) was identified by performing a T1 look-locker scan and selecting the TI with maximum nulling of healthy left ventricular myocardium. Free-breathing images were acquired using Spectral Presaturation with Inversion Recovery (SPIR) turbo field echo (TFE) sequence with respiratory navigator motion correction, a 12 degree flip angle and a 360 x 360mm field of view. Acquired voxel resolution was 1.8 x 1.8 x 3.6mm^2, which was reconstructed to 1.3 x 1.3 x 1.8mm^2. Acquisition window was 154ms and images were obtained in diastole. Typically, 80 slices were obtained to ensure full acquisition of the ventricular myocardium. Images were analysed, anonymised and exported using cvi42 version 5.14 (Circle Cardiovascular Imaging Inc, Calgary, Canada).

Anatomical assessment with ADAS

3D LGE images were imported into Automatic Detection of Arrhythmogenic Substrate (ADAS) (ADAS 3D, Galgo Medical, Barcelona, Spain) and analysed using a validated approach.[18,19] Endocardial and epicardial boundaries were contoured in a semi-automated fashion with manual adjustment where required by an expert operator. Once completed, the image segmentation was reviewed by two expert operators to ensure consistency.
The left ventricular (LV) myocardium was divided into nine sequential layers from endocardium to epicardium to generate nine 3D shells. Pixel signal intensity (PSI) maps were generated from the LGE images and projected onto each of the nine shells using a trilinear interpolation algorithm. Tissue was assigned based on signal intensity using the full-width half maximum (FWHM) approach with dense (core) scar being defined as > 50% (± 5%) maximal PSI and borderzone between 35% (± 5%) and 50% (± 5%) maximal PSI. Tissue with a PSI of less than 35% (± 5%) was designated as healthy. Conducting channels are identified based on prespecified tissue characteristics derived from the signal intensity maps and include either channels of borderzone between two areas of dense scar or between dense scar and an anatomical barrier (such as the mitral annulus). CC were defined as endocardial (in layers 10% - 30%), mid (40 - 60%) or epicardial (70 - 90%). Transmural channels were defined by presence in more than 75% of the total myocardial thickness. Surfaces from the AA were exported as .XML files for fusion with the EAM.

Heart digital twin model generation

Geometric model formation
The exported LGE-MRI images were reconstructed into geometrical models of the individual patient's ventricular myocardium. The images were resampled into short axis at an isotropic resolution of 0.35 x 0.35 x 0.35 mm. The myocardium was semi-automatically segmented as reported in previous publications.[1–3] In brief, landmark control points were placed along the left ventricular endocardium and epicardium using CardioViz3D.[4] From these points, the 3D myocardial wall geometry was

reconstructed using a method based on variational implicit functions interpolation which has been previously validated.[5] Dense scar and borderzone were identified in the myocardium using the full-width half-maximum methods. Areas of > 50% of the maximal signal intensity in the myocardium were assigned as dense scar. Areas of between 35% and 50% maximal signal intensity were designated as borderzone. All remaining areas are designated as healthy tissue. The 3D geometry of the infarcted areas is integrated into the geometric model. For a patient with an ICD *in situ*, additional processing was required. The ventricular geometry was extrapolated from the unaffected areas, through the region occluded by the ICD artefact. The myocardium within the ICD artefact was assumed to have normal tissue properties.

Next, from the reconstructed ventricular geometries, finite-element, tetrahedral meshes were generated using a commercial meshing software Materialize Mimics (Materialise NV, Leuven, Belgium) with a previously described meshing procedure.[6] On average, 4 million individual nodes form this mesh per patient, giving an average resolution of 400μm.[7] Finally, personalised fibre-orientation was applied to the computational mesh using a Laplace-Dirichlet rule-based approach which defines the transmural and apicobasal directions of the fibres for each point in the ventricles[8]. It then uses bi-directional spherical linear interpolation to assign fibre orientation which is based on a set of rules derived from previous histological analysis and diffusion tensor MRI data.[9–11]

Electrophysiological modelling

Once the ventricular mesh was created, cell and tissue electrophysiological properties were assigned based on the three different tissue types (healthy, borderzone and dense scar). Dense scar was considered electrically inert. Healthy areas were modelled based on previous modelling data by Tusscher.[12] Grey zone mechanics represent a modification of healthy ionic model based on previous patch clamp studies from cells taken from an infarct borderzone. The changes include a 62% reduction in peak sodium current, 69% reduction in L-type calcium current and a 70% and 80% reduction in the I_{Kr} and I_{ks} potassium currents respectively[9]. Compared with healthy tissue, these changes combine to give a reduced upstroke velocity of the action potential (6.7 vs 11.6 V/s), longer action potential duration (360 vs 310ms), and reduced peak AP amplitude (20 vs 35mV). Longitudinal and transverse conductivity in healthy tissue is set at 0.08 S/m and 0.00889 S/m respectively based on studies on human tissue. [13–16]. In the borderzone, there is a 90% reduction in transverse conductivity based on the observed reduction in connexin-43, reduced conduction velocity and other gap junction alterations observed in the post-infarct borderzone areas. [17]

Electrical propagation was simulated by solving a reaction-diffusion partial differential equation, which represents the spread of the electrical wavefront through the model, as well as the ordinary differential and algebraic equations representing myocyte membrane dynamics at each node in the mesh [18]. Simulation of electrical propagation using these equations was performed using the software package openCARP (https://opencarp.org) using a parallel computing system.[19] This software has been used to solve other computational EP problems in both animal and human subjects and has been validated in several publications[20–23].

VT induction protocol

Each patient's virtual heart was subjected to multi-site pacing in order to induce re-entrant rhythms. The aim is to simulate the degeneration of the electrical signal following a PVC into re-entrant VT within the diseased myocardium. Seven segments are used for the simulated pacing, which are derived from the 17-segment American Heart Association (AHA) model. If scar is present in that particular segment, the pacing location was projected to the scar area, in order to increase the chance of inducing a VT. Seven segments were chosen to balance the computational resources required for the modelling against the chances of inducing a VT, which increase with more pacing sites[24,25].

A pacing train (S1) of 6 beats was delivered at a 1 x 1 x 1mm spot at 600ms followed by an extrastimulus (S2) 300ms after S1. If this fails to capture, the S1-S2 interval is increased by 50ms until capture is achieved. Following capture of S2, the S1-S2 interval was shortened in 10ms intervals to find the shortest S1-S2 capture interval, which is then observed for the presence of re-entry. If no VT was induced with S2, a second (S3) or third (S4) extrastimulus was added. Sustained arrhythmia was defined as exhibiting two full rotations at a fixed location. Previous studies have shown that a longer observation period of up to 5 seconds does not reveal significantly more sustained VTs than a 2 second monitoring period[26]. Furthermore, the iterative in-silico ablation procedure makes sure that the heart digital twin is non-inducible of VT at the final iterations.

Catheter ablation protocol

Ablation was performed using the TactiCath Sensor Enabled catheter irrigated at 17ml/min. Ablation was performed at 30 – 50W targeting 60s per lesion targeting an impedance drop of > 10Ω, attenuation of abnormal potentials or until loss of capture during pacing at 10mA at 2ms.

Anatomical assessment and digital twin merging with electroanatomical map

The exported AA and DT model were sequentially merged with the EAM following completion of the ablation procedure. Merging used rigid coregistration of fiducial points including the coronary cusps, apex and the LV outflow tract and proximal ascending aorta between the EAM and the corresponding points on the MRI models and was performed by an independent expert. Ablation operators were blinded to the AA and DT outputs throughout the procedure.

Supplemental tables

Supplemental Table 1: Comparison of anatomical conducting channels vs DT primary predicted site characteristics

	AA (n = 42)	**DT primary sites (n = 62)**	**P – value**
Number per patient	2.33 (± 1.41)	3.44 (± 1.20)	0.02
Length per channel/site (mm)	45.5 (± 40.3)	26.92 (± 10.12)	0.005
Width per channel/site (mm)	8.08 (± 2.31)	7.34 (± 0.63)	0.05
Area per channel/site(cm^2)	4.17 (± 5.05)	1.96 (± 0.71)	0.007
Total area predicted per patient	9.94 (± 9.46)	6.74 (± 2.29)	0.18
Epicardial isthmus	21 (50.0%)	27 (43.5%)	0.55
No of AHA segments involved	2.40 (± 1.27)	1.50 (± 0.59)	< 0.001
EAM map density (points/cm^2)	42.3 (± 30.3)	39.7 (± 13.4)	0.76

AA = anatomical assessment, DT = digital twin, AHA = American Heart Association, EAM = electroanatomical map.

Supplemental figures

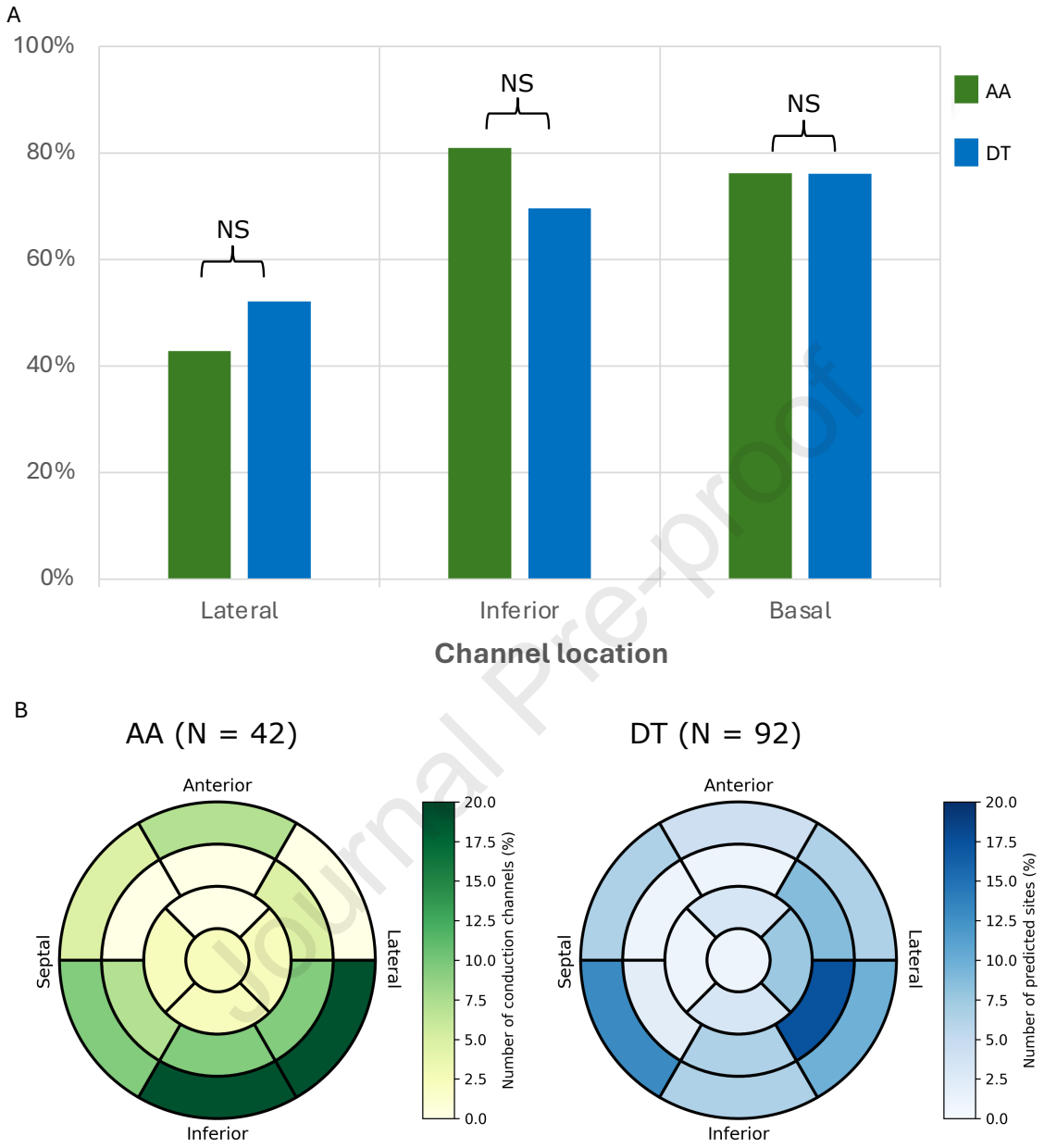

Supplemental Figure 1: Distribution of AA and DT targets

A - distribution of AA and DT targets, when categorised as lateral as opposed to septal, inferior as opposed to anterior and basal as opposed to apical. B – relative distribution of AA conducting channels and DT predicted sites by AHA segment. AA = anatomical assessment

Supplemental References

1. Sung E, Prakosa A, Zhou S, et al.: Fat infiltration in the infarcted heart as a paradigm for ventricular arrhythmias. Nature cardiovascular research, 2022; 1:933–945.
2. Sung E, Prakosa A, Aronis KN, et al.: Personalized Digital-Heart Technology for Ventricular Tachycardia Ablation Targeting in Hearts With Infiltrating Adiposity. Circulation: Arrhythmia and Electrophysiology, 2020; 13:E008912.
3. Zhang Y, Zhang K, Prakosa A, et al.: Predicting Ventricular Tachycardia Circuits in Patients with Arrhythmogenic Right Ventricular Cardiomyopathy using Genotype-specific Heart Digital Twins. eLife, 2023; 12.
4. Toussaint N, Mansi T, Delingette H, Ayache N, Sermesant M: An integrated platform for dynamic cardiac simulation and image processing: Application to personalised tetralogy of fallot simulation. EG VCBM 2008 - Eurographics Workshop on Visual Computing for Biomedicine, 2008; :21–28.
5. Prakosa A, Malamas P, Zhang S, et al.: Methodology for image-based reconstruction of ventricular geometry for patient-specific modeling of cardiac electrophysiology. Progress in Biophysics and Molecular Biology, 2014; 115:226–234.
6. Boyle PM, Ochs AR, Ali RL, Paliwal N, Trayanova NA: Characterizing the arrhythmogenic substrate in personalized models of atrial fibrillation: sensitivity to mesh resolution and pacing protocol in AF models. Europace : European pacing, arrhythmias, and cardiac electrophysiology : journal of the working groups on cardiac pacing, arrhythmias, and cardiac cellular electrophysiology of the European Society of Cardiology, 2021; 23:I3–I11.
7. Prassl AJ, Kickinger F, Ahammer H, et al.: Automatically generated, anatomically accurate meshes for cardiac electrophysiology problems. IEEE transactions on bio-medical engineering, 2009; 56:1318–1330.
8. Bayer JD, Beaumont J, Krol A: Laplace–Dirichlet Energy Field Specification for Deformable Models. An FEM Approach to Active Contour Fitting. Annals of Biomedical Engineering 2005 33:9, 2005; 33:1175–1186.
9. Arevalo HJ, Vadakkumpadan F, Guallar E, et al.: Arrhythmia risk stratification of patients after myocardial infarction using personalized heart models. Nature Communications, 2016; 7:1–8.
10. Deng D, Arevalo H, Pashakhanloo F, et al.: Accuracy of prediction of infarct-related arrhythmic circuits from image-based models reconstructed from low and high resolution MRI. Frontiers in Physiology, 2015; 6:282.
11. Bayer JD, Blake RC, Plank G, Trayanova NA: A novel rule-based algorithm for assigning myocardial fiber orientation to computational heart models. Annals of Biomedical Engineering, 2012; 40:2243–2254.
12. Ten Tusscher KHWJ, Noble D, Noble PJ, Panfilov A V.: A model for human ventricular tissue. American Journal of Physiology - Heart and Circulatory Physiology, 2004; 286:1573–1589.
13. Weiss DL, Seemann G, Keller DUJ, Farina D, Sachse FB, Dössel O: Modeling of heterogeneous electrophysiology in the human heart with respect to ECG genesis. Computers in Cardiology, 2007, pp. 49–52.
14. Hooks DA, Trew ML, Caldwell BJ, Sands GB, LeGrice IJ, Smaill BH: Laminar arrangement of ventricular myocytes influences electrical behavior of the heart. Circulation Research, 2007; 101.
15. Clayton RH, Panfilov A V.: A guide to modelling cardiac electrical activity in anatomically detailed ventricles [Internet]. Prog Biophys Mol Biol. 2008, pp. 19–43.
16. Poelzing S, Akar FG, Baron E, Rosenbaum DS: Heterogeneous connexin43 expression produces electrophysiological heterogeneities across ventricular wall. American Journal of Physiology - Heart and Circulatory Physiology, 2004; 286.

17. Yao JA, Hussain W, Patel P, Peters NS, Boyden PA, Wit AL: Remodeling of gap junctional channel function in epicardial border zone of healing canine infarcts. Circulation Research, 2003; 92:437–443.
18. Plank G, Zhou L, Greenstein JL, et al.: From mitochondrial ion channels to arrhythmias in the heart: Computational techniques to bridge the spatio-temporal scales. Philosophical Transactions of the Royal Society A: Mathematical, Physical and Engineering Sciences, 2008; 366:3381–3409.
19. Plank G, Loewe A, Neic A, et al.: The openCARP simulation environment for cardiac electrophysiology. Computer Methods and Programs in Biomedicine, 2021; 208:106223.
20. Bishop MJ, Rodriguez B, Qu F, Efimov IR, Gavaghan DJ, Trayanova NA: The Role of Photon Scattering in Optical Signal Distortion during Arrhythmia and Defibrillation. Biophysical Journal, 2007; 93:3714.
21. Rantner LJ, Arevalo HJ, Constantino JL, Efimov IR, Plank G, Trayanova NA: Three-dimensional mechanisms of increased vulnerability to electric shocks in myocardial infarction: Altered virtual electrode polarizations and conduction delay in the peri-infarct zone. The Journal of Physiology, 2012; 590:4537.
22. Rodríguez B, Li L, Eason JC, Efimov IR, Trayanova NA: Differences Between Left and Right Ventricular Chamber Geometry Affect Cardiac Vulnerability to Electric Shocks. Circulation research, 2005; 97:168.
23. Ashikaga H, Arevalo H, Vadakkumpadan F, et al.: Feasibility of Image-Based Simulation to Estimate Ablation Target in Human Ventricular Arrhythmia. Heart rhythm : the official journal of the Heart Rhythm Society, 2013; 10:1109.
24. Piccini JP, Hafley GE, Lee KL, et al.: Mode of induction of ventricular tachycardia and prognosis in patients with coronary disease: the Multicenter UnSustained Tachycardia Trial (MUSTT). Journal of cardiovascular electrophysiology, 2009; 20:850–855.
25. Buxton AE: Programmed ventricular stimulation: not dead. Circulation, 2014; 129:831–833.
26. Prakosa A, Arevalo HJ, Deng D, et al.: Personalized virtual-heart technology for guiding the ablation of infarct-related ventricular tachycardia. Nature Biomedical Engineering, 2018; 2:732–740.